

Electric Double Layer Effect on the Outer-Sphere Benzyl Halides Electro-Reduction Mechanism

Aleksandr S. Kramarenko,* Ivan Yu. Chernyshov, and Evgeny A. Pidko*



Cite This: *J. Phys. Chem. C* 2024, 128, 9462–9471



Read Online

ACCESS |



Metrics & More

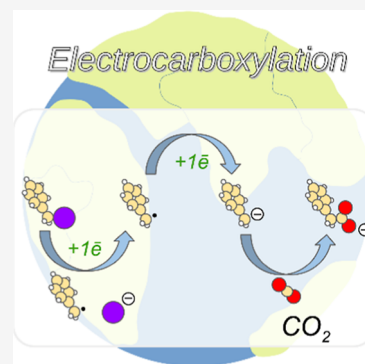


Article Recommendations



Supporting Information

ABSTRACT: Electrocatalytic reduction of organic halides and subsequent carboxylation are promising methods for the valorization of CO₂ as a C1 source in synthetic organic chemistry. The reaction mechanism underlying the selectivity and reduction mechanism of benzyl halides is highly dependent on the nature of the electrode material as well as the processes, composition, and structure of the liquid phase at the electrode–solution interface. Herein, we present a computational study on the influence of the electric double layer (EDL) on the activation of benzyl halides at different applied potentials over the Au (111) cathode. Using a multiscale modeling approach, we demonstrate that, under realistic electrocatalytic conditions, the formation of a dense EDL over the cathode hampers the diffusion of benzyl halides toward the electrode surface. A combination of classical molecular dynamics simulations and density functional theory calculations reveals the most favorable benzyl halide electro-carboxylation pathway over the EDL that does not require direct substrate adsorption to the cathode surface. The dense EDL promotes the dissociative reduction of the benzyl halides via the outer-sphere electron transfer from the cathode surface to the electrolyte. Such a reduction mechanism results in a benzyl radical intermediate, which is then converted to benzyl anions in the EDL via an additional electron transfer step.



INTRODUCTION

Electrocatalytic fixation of CO₂ is an effective method for chemical valorization of carbon dioxide, which could be readily achieved under mild conditions.¹ Among the various possible electrocatalytic processes, the electrochemical activation of benzyl halides and subsequent carbon dioxide fixation is considered a green and promising method for the synthesis of crucial carboxylic acid derivatives with a wide range of applications ranging from pharmaceuticals to fuel production.^{2–5}

The electrified interfaces are the key research object in electrocatalysis, in which the electrochemical potential determines the stability of adsorbed species and the electric double-layer (EDL) structure at the electrode surface. The computational description of the reactive environment and chemical transformations at the electrified interfaces during the electrocatalytic process is very challenging. Representative models need to account for both the electrochemical potential and the complex EDL environment. Most conventional computational approaches represent an electrochemical half-cell as a grand-canonical ensemble, where the number of electrons transferred is adjusted in line with the nature and chemical composition of the system.^{6–9} More advanced and realistic models include explicit solvent molecules and counterions to better represent the chemistry of the EDL at the expense of the drastically increased computational costs of the simulations.^{10–12} The computational demand of the electrochemical simulations can be substantially decreased by using various approximate methods,^{13–16} such as the computational

hydrogen electrode model introduced by Nørskov et al.,¹⁷ the Born–Haber cycles,¹⁸ and the Poisson–Boltzmann model.^{19,20}

Experimental studies^{21–24} demonstrate that electron transfer to benzyl halides is a complex process that is influenced by the interactions between the electrode surface and the reagents as well as their reduction products. As a result, the activity and selectivity of benzyl halide electrocarboxylation strongly depend on the electrode nature and the local solvent environment near the cathode surface.^{16,20} The cation species accumulated within the EDL near the cathode may stabilize the transition states of the electrocatalytic reactions.^{21,23,25} Furthermore, under applied bias, the concentration of such solvated cations near the cathode increases, resulting in a denser EDL and alternated solvation structure (Figure 1), which both may hamper the direct access of benzyl halide to the surface.^{16,26–28}

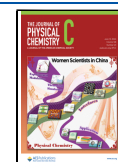
The reagents will become confined in a solvent cage, and an outer-sphere electron transfer (OSET) may occur as a homogeneous step over the EDL.¹⁶ In the OSET mechanism, an indirect transfer between the electrocatalyst and reagent occurs through the electrolyte without its chemisorption on the electrode surface. However, the role of such an indirect

Received: December 17, 2023

Revised: April 28, 2024

Accepted: May 21, 2024

Published: May 30, 2024



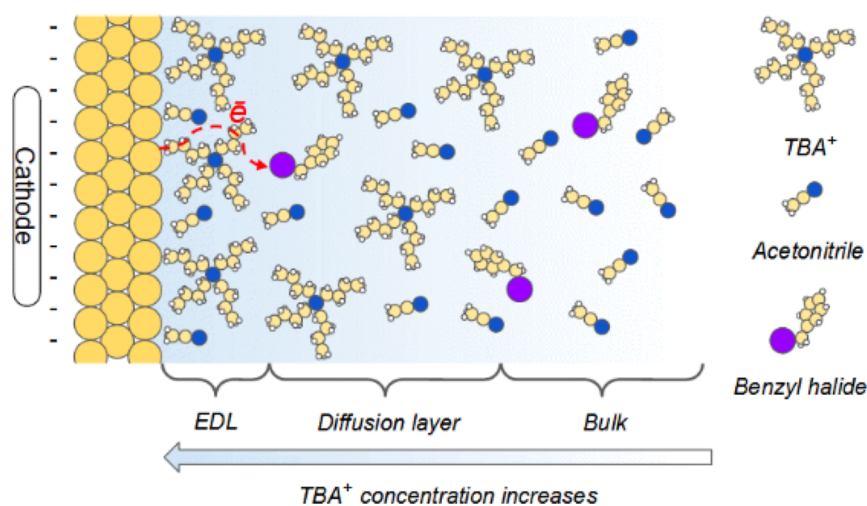


Figure 1. Electrode/electrolyte interface model for benzyl halide electrochemical reduction processes.

electroreduction mechanism in aryl halide carboxylation is moot. Molecular dynamics (MD) simulations provide a direct insight into the EDL structure, including crucial information about the respective concentration gradients, which, in turn, can be used to compute concentration-dependent thermodynamic parameters for various chemical reactions using advanced solvation models like COSMO-RS.^{29–32} Herein, we employed a multiscale modeling approach combining MD simulations to evaluate the concentrations of solution components near the electrode surface under electrochemically relevant reaction conditions and DFT calculations to investigate the thermodynamics of homogeneous electron transfer to benzyl bromide under realistic conditions and construct a detailed mechanism of reductive C–Hal bond cleavage.

METHODS

DFT Calculations. Thermodynamic parameters and geometries of all chemical species in this work were computed using the ORCA software package³³ with the combination of the B3LYP exchange–correlation functional^{34–37} and triple- ζ basis set (def2-TZVPP).³⁸ The Broyden–Fletcher–Goldfarb–Shanno scheme was used in geometry optimizations with a convergence criterion based on a maximum relaxation force of 0.015 eV/Å. The SCF convergence was assumed when the energy difference between the adjacent electronic optimization steps was below to 10^{-8} hartree. The CPCM solvation model was used to account for the bulk solvent effects on the reaction path and their energetic contribution to the overall reaction.³⁹ The values of the standard reduction potentials (SRP) of the one-electron transfer step to benzyl halides in acetonitrile medium were computed using simplified thermodynamic cycles.^{14,15,23} For each half-reaction, the free Gibbs energy and corresponding SRPs were calculated according to

$$\Delta G_r^0 = \Delta G_{r(g)}^0 + \Delta G_{r(sol)}^0 + \Delta mRT \ln(22.46) \quad (1)$$

where $\Delta G_r^0(g)$ stands for the Gibbs free energy change of the reaction in the gas phase, and $\Delta G_r^0(sol)$ is the free energy change of solvation ($\Delta G_r^0(sol)$). The correction term $\Delta mRT \ln(22.46)$ refers to the change in the number of moles of solvated species from 1 M/L in the gas phase to 1 M/L in solution. For the reaction of dissociative electron-transfer $\Delta m = 1$, the resulting free energy is related to the SRPs by eq 2⁴⁰

$$E^0 = \frac{-\Delta G_r^0}{nF} - E_{ref}^0 \quad (2)$$

where E_{ref} is the SRP of the reference electrode, which is 4.422 V for the saturated calomel electrode (SCE) in acetonitrile solution.¹⁴ eq 2 indicates the equilibrium electrode potential for a given transformation. Our decision to employ the B3LYP functional was guided by prior investigations, where reduction potentials for a diverse array of organic halides were calculated using the G3(MP2)-RAD(+)//B3LYP/6-31+G(d) and MRMP2/6-31+G(d)//MCSCF/6-31+G(d) levels of theory.^{14,22} By comparing our findings with these studies and experimental reduction potentials^{23,41,42} for the species examined, we noted that the disparities in reduction potentials fell within the error margin of the DFT approach and did not exceed 0.2 eV.

To evaluate the solvation effect of an electric double layer (EDL) with a high concentration of supporting electrolyte cations on the reaction thermodynamics, we used the COSMO-RS solvation model⁴³ implemented in COSMOTermX (version 19.0.5) computational package. The statistical approach of the model allows for the investigation of the solvation effects in complex multicomponent solutions. In this model, solvent–solute interactions are expressed as a local contact energy and quantified by the local polarization densities of the contacting molecular surfaces,^{32,44,45} and therefore solvation energies can be calculated even in charged solutions. Solvation energies for the electro-reduction intermediates were calculated in pure acetonitrile and solution mixtures with tetrabutyl ammonium cation mole fractions ranging from 0 to 0.9, representing the concentration gradient from the bulk solution to the dense part of the EDL, especially in the reaction region mentioned above. The correction for solvation energy of a reaction species was calculated by

$$G_{solv} = G_{CPCM} - G_{COSMO-RS} + G_{Model} \quad (3)$$

where G_{CPCM} —is the solvation free energy of a given species in ideal acetonitrile solution obtained within the CPCM solvation model, $G_{COSMO-RS}$ —is the solvation free energy of a species in pure acetonitrile (1 M) obtained by the COSMO-RS solvation model, and G_{Model} —is the solvation free energy of a given species in model multicomponent concentrated solution obtained by the COSMO-RS solvation model. The solvation

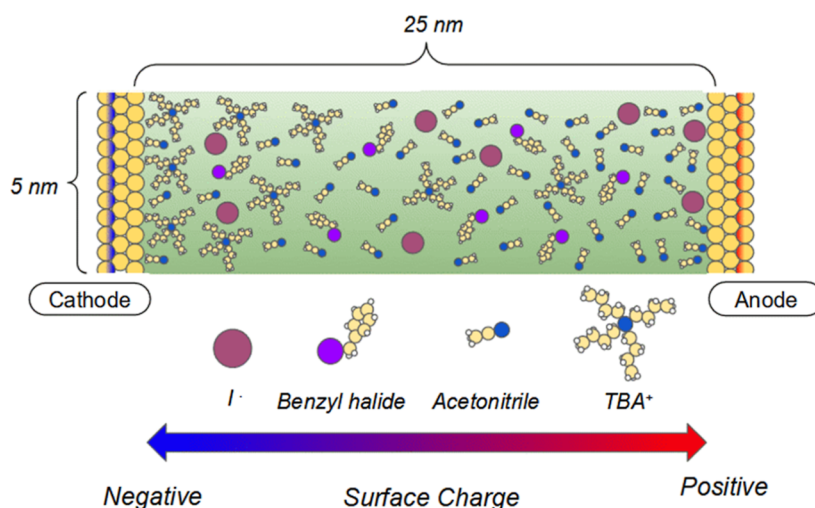


Figure 2. Schematic representation of the MD simulation cell.

energies of each species were computed and then used to determine the change in the solvation energy term, incorporated into eq 1. Previously optimized geometries of reaction species in ORCA software were used to generate COSMO-files using the Turbomole software (version 4.4.1) together with the combination of B3LYP exchange–correlation functional and triple- ζ basis set (def2-TZVPP).

Molecular Dynamic Simulations. Concentration distributions of the solution components in the EDL region can reveal the solvation structure of benzyl halides in the EDL. MD simulations were performed using the GROMACS package (version 2021.5).^{46,47} In this study, we used the Au (fcc) facet to simulate electrode surfaces. The electrode surfaces are constructed by using bulk metal structures extracted from Crystallography Open Database⁴⁸ (COD) (materials id 1100138).⁴⁹ Metal slabs with an electrolyte bulk that consisted of TBA⁺, I[−], BnBr, and MeCN molecules were constructed using the GROMACS insert-molecules tool. The concentrations are set to reproduce the voltametric experimental conditions^{4,21,41} namely, 0.2 M for TBA⁺, 0.2 M for I[−], 0.1 M for benzyl bromide. The simulations are carried out using a supercell measuring $4.995 \times 4.326 \times 35$ nm for Au electrodes, to prevent the influence of boundary effects and adequately simulate the adsorption of large cations on the electrode surface. The periodic boundary conditions were applied in the *x* and *y* directions, whereas in the *z* direction, the system remained nonperiodic. A constant charge method^{16,28} was used to simulate externally applied potential by adding negative and positive charge behind the electrode slabs (Figure 2).

The magnitude of the electric field on the cathodic and anodic surfaces due to the polarization induced by ghost charges was in the 0–10 V/nm range. The interatomic interactions between the components were modeled via the Lennard-Jones (LJ) potential with a cutoff of 1 nm. The cross-terms were obtained using the Lorentz–Berthelot mixing rule. The force field files for use with the GROMACS package are presented in [Supporting Information](#). Acetonitrile was modeled using a flexible six-site potential model introduced by Kowsari and Tohidifar.⁵⁰ The LJ parameters for BnBr, TBA⁺, and I[−] were taken from the literature.^{51–54} The van der Waals interactions of the solute with Au (111) were represented by Lennard-Jones potential described by Heinz et al.⁵⁵ Several studies have demonstrated that these parameters can qualitatively replicate interactions

between the metal surface and the solution interface,^{28,56–62} while the Lennard-Jones parameters for interactions in solution effectively capture physical phenomena in the bulk.

The long-range interactions were calculated with the particle-mesh Ewald (PME) method. The chemical bonds with hydrogen atoms were constrained using the LINKS algorithm,⁶³ whereas all other types of bonds were treated using harmonic bond approximation. The temperature of the simulation systems was maintained using a modified Berendsen thermostat at a value of 300 K.

The preparation of the simulation system included a 10 ns simulation of bulk electrolyte with constant a number of particles, cell volume, and temperature (NVT) solution, followed by a 10 ns simulation with a constant number of particles, pressure, and temperature (NPT) solution. The resulting solution structures were placed between two parallel metal plates and annealed at 150, 650, 600, 550, 500, 450, 400, 350, and 300 K for 3 ns each. Subsequently, the resulting configuration again was equilibrated for 10 ns, followed by a production run of 90 ns.

Electrode Potential Distribution. The total electrostatic potential was calculated using the following equation²⁸

$$\varphi(z) = \varphi_{\text{sol}}(z) + \varphi_{\sigma}(z) \quad (4)$$

where $\varphi_{\sigma}(z)$ is the potential of the external electric field created by the charge on the electrode surface and can be computed according to the eq 5

$$\varphi_{\sigma}(z) = \sigma \frac{4\pi}{\epsilon} \int_0^z dz \quad (5)$$

where *z* is the distance from the electrode surface, ϵ is the dielectric permittivity of the solvent, and $\varphi_{\text{sol}}(z)$ is the electrostatic potential induced by the solution in response to an external electric field. This term can be calculated by integrating the eq 6

$$\varphi_{\text{sol}}(z) = \frac{4\pi}{\epsilon} \int_0^z (z - z') \rho(z') dz' \quad (6)$$

where $\rho(z')$ is the charge density distribution along the normal direction of the simulation cell. [Figure S3](#) represents the charge distribution for the studied systems. The final electrostatic potential drop for EDL can be calculated by eq 7.

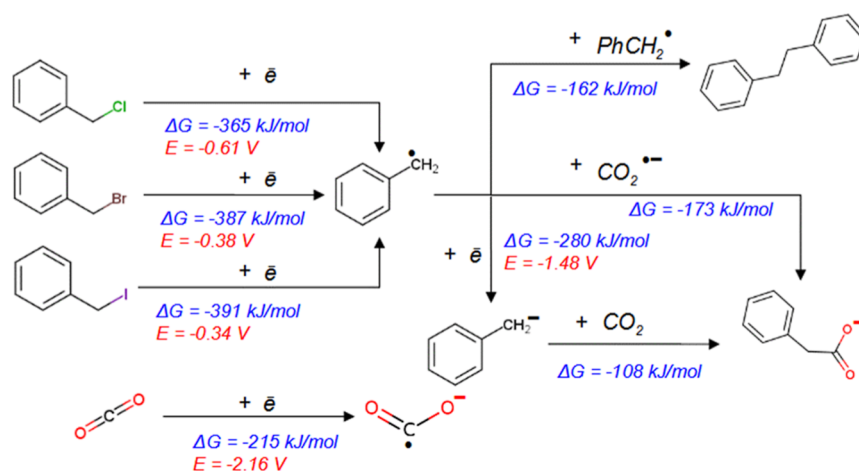


Figure 3. Possible pathway of benzyl halide electrochemical carboxylation and thermodynamic effects of elementary steps. Reduction potentials are referenced to the SCE of 4.422 V.

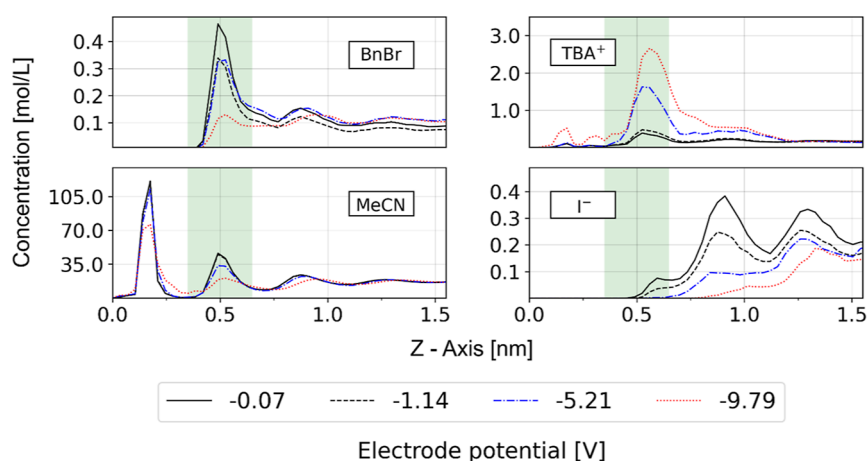


Figure 4. Components distribution along the Z—direction of the simulation cell at different electrode potentials. The cathode is placed at 0.0 nm.

$$U = \Phi_{\text{electrode}} - \Phi_{\text{bulk}} \quad (7)$$

where $\Phi_{\text{electrode}}$ represents the electrostatic potential on the electrode surface, and Φ_{bulk} denotes electrostatic potential in the bulk solution.

RESULTS AND DISCUSSION

Bulk Electrolysis Simulation. To check our hypothesis on the potential role of the outer-sphere electron transfer in benzyl halide electroreduction, we first computationally evaluated the thermodynamic parameters of the overall reaction by DFT calculations with the implicit solvation model. The main results are summarized in Figure 3.

Figure 3 displays the computed values of Gibbs free energy change for both the electrochemical and thermochemical phases of the process, alongside the SRPs for the electrochemical stages. The electrochemical initiation of benzyl halides involves the reductive cleavage of the C–Hal bond, leading to the generation of free benzyl radicals and corresponding halide anions.²³ The free energy associated with this step is notably influenced by the leaving anion, decreasing in the order BnCl > BnBr > BnI. This reduction is accompanied by a continuous shift toward less negative SRP values in the opposite order, a trend explained by the diminishing C–Hal bond dissociation energy⁶⁴ in the same order. The subsequent reduction of benzyl radicals is an energetically less favorable step, with a free energy change that is

approximately 100 kJ/mol more positive than the initial electron transfer. This results in a more negative reduction potential of -1.48 V vs SCE, consistent with the experimentally determined SRP for the second electron transfer of -1.43 V vs SCE.^{4,25} Beyond potentials of -1.5 V,^{4,21,25} this reaction sequence would yield 1,2-diphenylethane as the primary product. The generation of the target phenyl acetate ion can proceed through two alternative reaction channels, differing in the active reduced species. The electroreduction of CO_2 to $\text{CO}_2^{\bullet-}$, followed by its reaction with the benzyl radical, is more energetically favorable (-173 kJ/mol) than the alternative path, where the organic radical is first reduced, followed by the reaction of CO_2 with the benzyl anion (-108 kJ/mol). However, the formation of highly reactive $\text{CO}_2^{\bullet-}$ species is a highly activated process characterized by an extremely low computed SRP of -2.16 V vs SCE. The homogeneous reductive activation of benzyl halides toward benzyl ion, followed by its coupling with molecular CO_2 , is -108 kJ/mol and avoids highly unfavorable steps. This suggests the principal possibility of an outer-sphere reduction mechanism, particularly evident in situations where diffusion toward the cathode surface is hindered under electrochemical conditions.

EDL Structure near the Electrodes. To investigate the accessibility of the cathode surface to the benzyl halide molecules under the electroreduction conditions, we studied

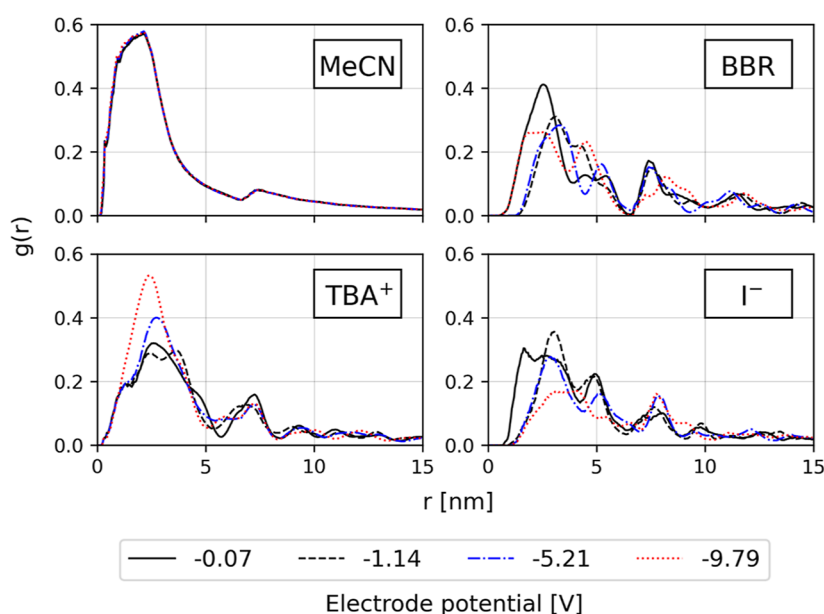


Figure 5. Pair-correlation function between the electrode surface and the center of mass of acetonitrile, benzyl bromide, tetrabutyl ammonium, and iodide anions at different electrode potentials.

the distribution of the model solution components exposed to the applied potential with various intensities by MD simulation.

Figure 4 represents the EDL composition at different electrode potentials and describes the formation of a solvation shell on the cathode surface, where the green region in the figure denotes the possible reaction region due to the location of the benzyl bromide concentration peak. The appearance of three successive peaks originating from MeCN within 1 nm of the electrode surface indicates the formation of tightly stacked layers. These layers demonstrate a consistent decrease in MeCN concentration influenced by the applied electric field. Furthermore, a slight shift in the peaks toward a greater distance from the electrode is observed, and this is ascribed to the influence of electrode polarization on solvent orientation.

A comparable impact of the electric field was noted on the opposing side of the simulation cell, near the anode surface, where there was a sustained reduction in the BnBr concentration. This observation is illustrated in the SI (Figure S1).

Aside from analyzing the concentration profile within the EDL, we also explored the pair-correlation between the cathode surface and the center of mass (COM) of individual solution components to characterize the EDL structure at different electrode potentials.

The cathode-acetonitrile pair-distribution function does not depend on the electrode potential, with the first solvation shell located within 5 nm of the cathode surface. The pair-correlation function for benzyl bromide (BBR) changes substantially with increasing potential and is consistently shifted to longer distances. At -0.07 V, the peak of the pair-correlation function is observed around 2.5 nm. At more negative potentials, it becomes less likely to locate benzyl bromide near the electrode surface in line with the concentration profile of BBR in the EDL (Figure 4). This could be attributed to the diminishing adsorption energy of benzyl bromide on the electrode surface due to surface polarization and the adsorption of charged species, which push the reactant molecules away into the bulk solution. The distribution of the TBA⁺ and I⁻ ions also depends notably on the electrode potential (Figure 5), with their pair-

correlation functions showing trends similar to those of the respective concentration profiles presented in Figure 4.

The concentration profiles of BnBr in the first and second solvation shells, as observed in Figure 4, can be attributed to both thermodynamic restrictions of the adsorption process and kinetic limitations that hinder adsorption events. Addressing the kinetic aspect involves employing sufficiently long simulation times, while assessing the thermodynamics of the adsorption process can be achieved through potential mean force (PMF) analysis, as depicted in Figure 6. Our analysis indicates that at

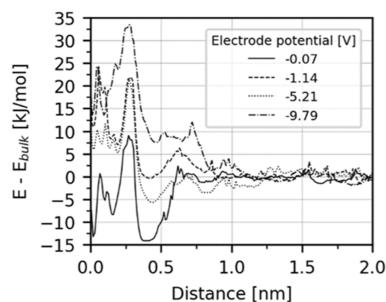


Figure 6. Potential of the mean force of benzyl bromide at different electrode potentials. PMF is calculated between the center of mass of the electrode and benzyl bromide. The electrode surface is uniformly placed at 0 nm.

low electrode potentials, benzyl bromide molecules may indeed reach the surface and become surface-adsorbed species. However, this process necessitates overcoming a free energy barrier of approximately 25 kJ/mol, with slight dependence on the applied potential. Additionally, we noted that the energy well for the adsorbed species is comparable to that found at a distance of 0.5 nm from the surface. This observation may elucidate the absence of adsorbed benzyl bromide on the electrode surface during the primary simulation. Furthermore, the application of an external electric field generated by the electrode reduces the free energy of the adsorbed state, making it less favorable by approximately 20 kJ/mol. These findings suggest that in real

systems, both thermodynamic and kinetic limitations hinder access of BnBr to the electrode surface.

Similarly, the free energy of benzyl bromide in the well situated 0.5 nm from the electrode also decreases, albeit at a slower rate. This phenomenon makes this region more favorable for the accumulation of benzyl bromide, with the desorption process of benzyl bromide becoming dominant. Applied electric field changes the solvent orientation from lateral to perpendicular (Figure 7). Such preference in orientation allows to maximize van der Waals interactions with the electrode surface and reduces the influence of the electric field mode.^{27,65–67}

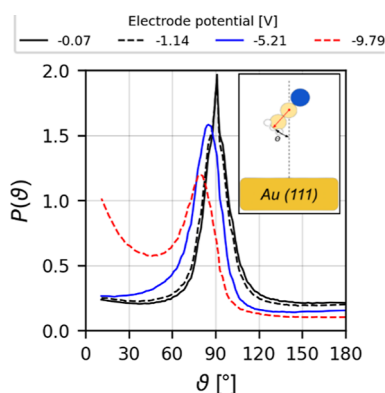


Figure 7. Angle distribution function of the solvent molecules in the first solvation layer with respect to the surface normal.

The increase of electrode surface polarization leads to the accumulation of TBA⁺ ions near the cathode, while I[−] ions show a steady decrease in the cathodic EDL. The bulkiness and conformational flexibility of *n*-Bu₄N cations and their high concentration in EDL, in combination with the perpendicular orientation of solvent molecules, hamper the accessibility of the BnBr reagent molecules, resulting in the decreasing BnBr concentration of BnBr in the green region with the increasing electric field strength. The accumulation of reactants in the EDL away from the electrode surface results in a reduction of adiabatic electronic coupling between the initial and final reaction states.^{68–70} Consequently, the initial state needs to traverse the transition state multiple times, leading to a decrease in the reaction rate. This phenomenon has been demonstrated and analyzed in recent studies conducted by Rybkin and colleagues using a high level of theory, particularly in the context of carbon dioxide electroreduction in aqueous solutions.^{71,72} Nevertheless, it is plausible that a similar nature of this effect may be observed for nonaqueous solvents, such as acetonitrile. This can describe a large potential difference between the experimental peak potential and reduction potential of -1.45 and -1.08 V vs SCE for BnCl and BnBr, respectively.⁴² Figure 8 summarizes the calculated diffusion coefficients of the model solution components. Computational results unveil that the applied electric field and surface polarization slightly affect the mobility of acetonitrile in the EDL, whereas charged species show a significant increase of the self-diffusion coefficients, indicating enhanced molecular exchange between bulk and EDL. The formation of the dense solvation layer composed of large cations, solvent, and benzyl bromide imposes diffusion limitations on the molecular transport between EDL and bulk solution, resulting in decreased reagent concentration in the EDL and its accumulation in the second solvation shell.

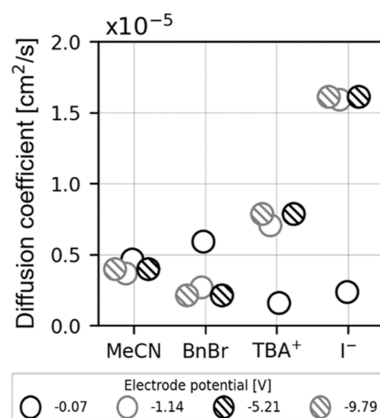


Figure 8. Self-diffusion coefficients of the solution components in the *z* direction in the intermediate layer between the EDL and bulk solution (0–1.5 nm from the cathode).

Additionally, the intensity of the electric field has a subtle impact on the extent of molecular mobility within the confined space of the narrow EDL region, spanning approximately 1.5 nm. Consequently, when an electric field is applied, the solution components tend to migrate at a similar rate, regardless of the strength of the electric field.

Figure 9 represents the electrostatic potential profile along the simulation cell, revealing the change of electrode potentials.

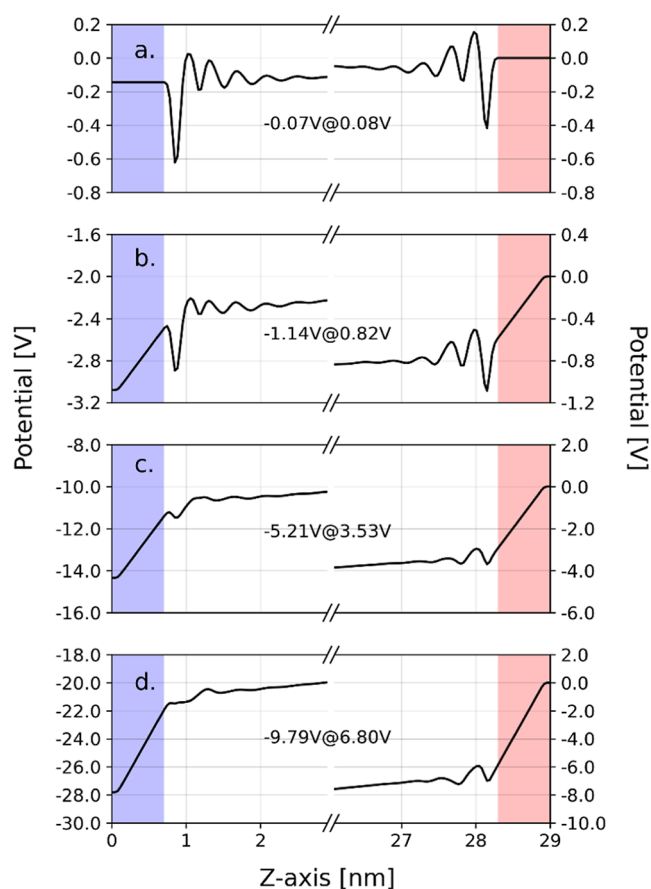


Figure 9. Electrostatic potential distribution along the simulation cell. The red and blue sections denote the anode and cathode, respectively. The applied potentials at the cathode and the anode are labeled separately in the figure.

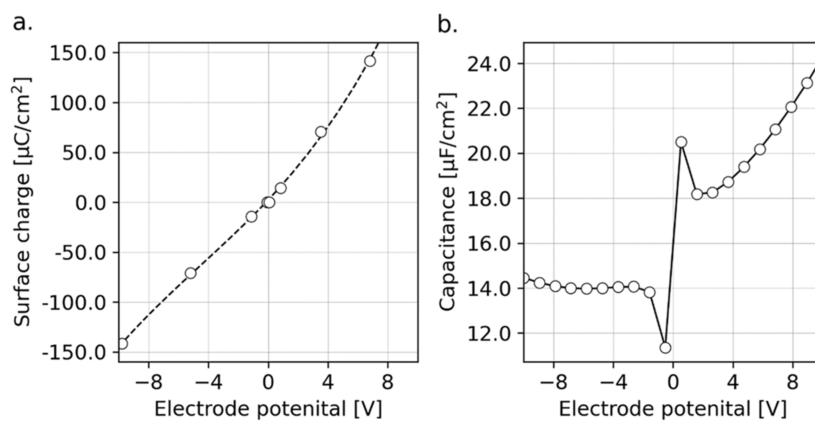


Figure 10. Relation between electrode charge density and potential drop across the EDLs adjacent to the electrodes (a) together with the EDL capacitance with different surface charge densities (b).

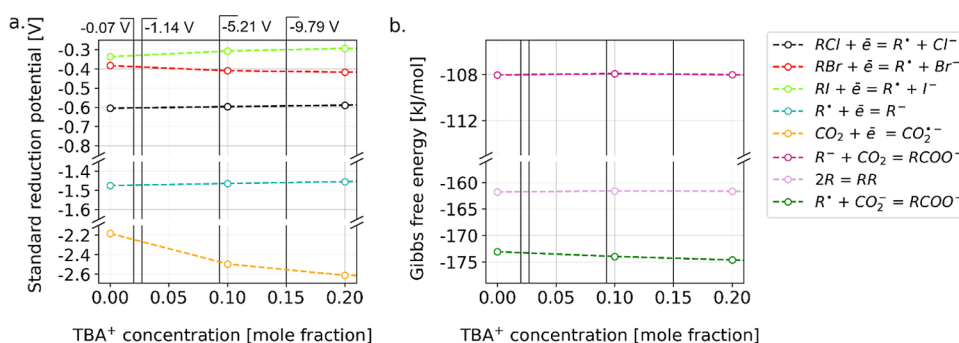


Figure 11. SRP (a) of the electrochemical steps of the electrocarboxylation process and Gibbs free energy change (b) of the corresponding thermochemical stages. Solid lines denote the TBA⁺ concentration obtained from MD simulations at various electric field intensities. SRPs are referenced to the SCE.

Figure 9 accurately depicts the location of the first potential peak between 0.6 and 1 nm near the cathode, corresponding to the first solvation layer in Figure 4. Similar observations regarding the location of potential peaks can be seen at the anode, as shown in Figure S1. The electrostatic potentials at both the anode and cathode (Figure 9) exhibit oscillations in the EDL region (within 1.5 nm from the electrode surface), gradually decaying to a linearly increasing potential in the bulk region. The potential drop induced by the adsorption of ions and solvent molecules decreases with the increase in electrode surface charge, which, in turn, limits the adsorption of benzyl bromide to the electrode surface. To compute the capacitance of the EDLs, we first fitted the electrode potential–surface charge correlation and then computed the EDL capacitance via eq 8,^{28,61}

$$C_{\text{edl}} = \frac{\sigma}{U_{\text{electrode}}} \quad (8)$$

where σ denotes the surface charge of the corresponding electrode, and $U_{\text{electrode}}$ is the electrode potential. The results are summarized in Figure 10.

Figure 10a shows the dependence of the surface charge on the electrode potential, which was utilized to compute the correlation for the EDL capacitance (Figure 10b). The latter is found to be sensitive to the electrode charge. At high positive potentials, it presents a bell-shaped curve with two wings, one of which shows an increase in capacitance due to anion adsorption on the anode surface. At negative potentials, the EDL capacitance stays relatively constant. We hypothesize that this

could be due to the rapid saturation of the EDL due to the large size of the cations and their flexible structure, which increases the EDL width and slows the capacitance growth. The magnitude of the EDL capacitance obtained in our simulation is in good agreement with the experimental values, typically falling in the range of 20 to 25 $\mu\text{F}/\text{cm}^2$,⁷³ evidencing the sufficient accuracy of our MD methodology to effectively capture the essential characteristics of the EDLs.

EDL Effects on Reaction Thermodynamics. The MD simulation reveals the formation of substantial concentration gradients near the cathode surface and, in particular, the accumulation of TBA⁺ cations near the negatively charged electrode under the conditions of electrochemical reactions. The resulting changes in the local solution composition may affect the free energy change of the elementary reaction steps.^{74,75} Certain typical electrochemical systems exhibit a pronounced dependence on the concentration of the supporting electrolyte, as observed in cases like ferrocene/ferrocenium.^{76–78} Therefore, we next investigated the influence of the composition of the EDL on the free energies of the electrochemical reaction by DFT calculations with the implicit COSMO-RS solvation model. Figure 11 shows the influence of EDL composition on the thermodynamics of the electrochemical and thermochemical steps of the process.

Figure 11 depicts the influence of the EDL composition on both the electrochemical and thermochemical aspects of the process. While a high concentration of TBA⁺ cations appears to have minimal impact on the chemical steps within the studied electrode potential range, the concentration of the supporting

electrolyte may notably affect the electrochemical steps. The SRP of CO₂ for producing CO₂⁻ substantially decreases with an increasing cation concentration. Notably, at an electrode potential of -9.79 V, the CO₂ reduction potential drops to around -2.50 V vs SCE, indicating a significant effect of 0.30 V. This suggests that the effective formation of ion pairs in the electrolyte induces a shift in the redox potential by altering the equilibrium concentration of active species.^{78–80} Benzyl halides exhibit varying responses to changes in TBA cation concentration following the sequence of BnI > BnBr > BnCl. While the SRP of BnCl remains constant (-0.61 V vs SCE) across the potential range, the SRP of BnBr shifts toward more negative values, from -0.38 V in pure acetonitrile to -0.42 V vs SCE at TBA⁺ 0.1 mole fraction, rendering the process less favorable. In contrast, BnI shows a positive shift from -0.34 V vs SCE in pure acetonitrile to -0.30 V vs SCE at an electrode potential of approximately -5 V, slightly enhancing thermodynamic feasibility. This highlights the significant role of the supporting electrolyte in reaction thermodynamics, which is influenced by the nature of the cation. Moreover, the magnitude of the response correlates with the generated halide anion and the strength of the C–Hal bond.

CONCLUSIONS

In the current study, we have explored the electrochemical activation and reduction mechanisms of some organic halides and their subsequent electrocarboxylation. Following our multiscale approach, we first performed bulk electrolysis simulation in order to investigate the energetic parameters of carboxylation elementary steps in acetonitrile media. The combination of multiple solvation models revealed only a very minor effect of the condensed EDL part under various applied biases on the energetics of most of the possible elementary reaction steps, except for the CO₂ reduction, where the additional TBA⁺ cations in the EDL change the SRP by up to 0.4 V. Our reaction scheme considers two possible scenarios of target phenyl carboxylate ion formation. The reaction thermodynamics analysis unveils the possibility of simultaneous reactions of radical coupling and benzyl anion reactions with the CO₂ molecules due to the close values of reaction energy, which is proved by previously reported experimental data.

Hence, in order to investigate our proposed OSET activation of benzyl halides, we simulated a complex multicomponent electrolyte-cathode system under various applied potentials. Density profile analysis revealed the formation of a dense EDL layer consisting mainly of dense layers of acetonitrile molecules and positively charged ions with irregular shapes and highly distributed charges, which reduces the diffusion ability of benzyl bromide molecules between the EDL and bulk solution. Eventually, all of these simultaneously occurring processes reduce the concentration of BnBr molecules in the EDL. As a result, the BnBr concentration on the electrode surface tends to zero, and the interaction with the surface is described by the solvent medium and might be completely absent. The outcomes suggest that in real-world systems, both thermodynamic and kinetic limitations hinder BnBr access to the electrode surface. In this case, the OSET might be an additional mechanism to produce benzyl radical, which is in line with the dissociative bond-breaking step for the benzyl halides.

ASSOCIATED CONTENT

Supporting Information

The Supporting Information is available free of charge at <https://pubs.acs.org/doi/10.1021/acs.jpcc.3c08224>.

Component distribution near the anode, electric field distribution along the cell, and charge density distribution along the cell (PDF)

Force field parameters, molecular structures, and topologies (ZIP)

AUTHOR INFORMATION

Corresponding Authors

Aleksandr S. Kramarenko – *International Institute “Solution Chemistry of Advanced Materials and Technologies”, ITMO University, Saint Petersburg 191002, Russia; Present Address: Institute for Chemical Technology and Polymer Chemistry, Karlsruhe Institute of Technology, Engesserstrasse 18, 76131 Karlsruhe, Germany; Email: aleksandr.kramarenko@partner.kit.edu*

Evgeny A. Pidko – *Inorganic Systems Engineering Group, Department of Chemical Engineering, Faculty of Applied Sciences, Delft University of Technology, Delft 2628 CN, The Netherlands; orcid.org/0000-0001-9242-9901; Email: e.a.pidko@tudelft.nl*

Author

Ivan Yu. Chernyshov – *Inorganic Systems Engineering Group, Department of Chemical Engineering, Faculty of Applied Sciences, Delft University of Technology, Delft 2628 CN, The Netherlands; orcid.org/0000-0002-4452-2025*

Complete contact information is available at: <https://pubs.acs.org/doi/10.1021/acs.jpcc.3c08224>

Author Contributions

The manuscript was written through contributions of all authors. All authors have given approval to the final version of the manuscript.

Notes

The authors declare no competing financial interest.

ACKNOWLEDGMENTS

A.S.K. thanks the Russian Science Foundation (Project no. 20-73-10165) for support. I.Yu.C. and E.A.P. thank The Netherlands Organization for Scientific Research (NWO) for access to SurfSARA supercomputer resources during the execution of this project in 2020–2021.

REFERENCES

- (1) Gao, D.; Arán-Ais, R. M.; Jeon, H. S.; Roldan Cuenya, B. Rational Catalyst and Electrolyte Design for CO₂ Electroreduction towards Multicarbon Products. *Nat. Catal.* **2019**, *2* (3), 198–210.
- (2) Mena, S.; Sanchez, J.; Guirado, G. Electrocarboxylation of 1-Chloro-(4-Isobutylphenyl)Ethane with a Silver Cathode in Ionic Liquids: An Environmentally Benign and Efficient Way to Synthesize Ibuprofen. *RSC Adv.* **2019**, *9* (26), 15115–15123.
- (3) Banerjee, A.; Dick, G. R.; Yoshino, T.; Kanan, M. W. Carbon Dioxide Utilization via Carbonate-Promoted C-H Carboxylation. *Nature* **2016**, *531* (7593), 215–219.
- (4) Medvedev, J. J.; Medvedeva, X. V.; Li, F.; Zienchuk, T. A.; Klinkova, A. Electrochemical CO₂ Fixation to α -Methylbenzyl Bromide in Divided Cells with Nonsacrificial Anodes and Aqueous Anolytes. *ACS Sustainable Chem. Eng.* **2019**, *7* (24), 19631–19639.

- (5) Matthesen, R.; Fransaer, J.; Binnemans, K.; De Vos, D. E. Reductive Carboxylation: Towards Sustainable and Efficient Synthesis of Valuable Carboxylic Acids. *Beilstein J. Org. Chem.* **2014**, *10* (1), 2484–2500.
- (6) Steinmann, S. N.; Michel, C.; Schwiedernoch, R.; Sautet, P. Impacts of Electrode Potentials and Solvents on the Electroreduction of CO₂: A Comparison of Theoretical Approaches. *Phys. Chem. Chem. Phys.* **2015**, *17* (21), 13949–13963.
- (7) Xiao, H.; Cheng, T.; Goddard, W. A.; Sundararaman, R. Mechanistic Explanation of the pH Dependence and Onset Potentials for Hydrocarbon Products from Electrochemical Reduction of CO on Cu (111). *J. Am. Chem. Soc.* **2016**, *138* (2), 483–486.
- (8) Goodpaster, J. D.; Bell, A. T.; Head-Gordon, M. Identification of Possible Pathways for C-C Bond Formation during Electrochemical Reduction of CO₂: New Theoretical Insights from an Improved Electrochemical Model. *J. Phys. Chem. Lett.* **2016**, *7* (8), 1471–1477.
- (9) Wang, J.-S.; Zhao, G.-C.; Qiu, Y.-Q.; Liu, C.-G. Strong Boron-Carbon Bonding Interaction Drives CO₂ Reduction to Ethanol over the Boron-Doped Cu(111) Surface: An Insight from the First-Principles Calculations. *J. Phys. Chem. C* **2021**, *125* (1), 572–582.
- (10) Ou, L.; Chen, J.; Chen, Y.; Jin, J. Mechanistic Study on Cu-Catalyzed CO₂ Electroreduction into CH₄ at Simulated Low Overpotentials Based on an Improved Electrochemical Model. *Phys. Chem. Chem. Phys.* **2019**, *21* (28), 15531–15540.
- (11) Luo, W.; Nie, X.; Janik, M. J.; Asthagiri, A. Facet Dependence of CO₂ Reduction Paths on Cu Electrodes. *ACS Catal.* **2016**, *6* (1), 219–229.
- (12) Cheng, T.; Xiao, H.; Goddard, W. A. Free-Energy Barriers and Reaction Mechanisms for the Electrochemical Reduction of CO on the Cu(100) Surface, Including Multiple Layers of Explicit Solvent at pH 0. *J. Phys. Chem. Lett.* **2015**, *6* (23), 4767–4773.
- (13) Ludwig, T.; Gauthier, J. A.; Dickens, C. F.; Brown, K. S.; Ringe, S.; Chan, K.; Nørskov, J. K. Atomistic Insight into Cation Effects on Binding Energies in Cu-Catalyzed Carbon Dioxide Reduction. *J. Phys. Chem. C* **2020**, *124* (45), 24765–24775.
- (14) Lin, C. Y.; Coote, M. L.; Gennaro, A.; Matyjaszewski, K. Ab Initio Evaluation of the Thermodynamic and Electrochemical Properties of Alkyl Halides and Radicals and Their Mechanistic Implications for Atom Transfer Radical Polymerization. *J. Am. Chem. Soc.* **2008**, *130* (38), 12762–12774.
- (15) Huang, Y.-F.; Wu, D.-Y.; Wang, A.; Ren, B.; Rondinini, S.; Tian, Z.-Q.; Amatore, C. Bridging the Gap between Electrochemical and Organometallic Activation: Benzyl Chloride Reduction at Silver Cathodes. *J. Am. Chem. Soc.* **2010**, *132* (48), 17199–17210.
- (16) Sinha, V.; Khramenkova, E.; Pidko, E. A. Solvent-Mediated Outer-Sphere CO₂ Electro-Reduction Mechanism over the Ag₁₁₁ Surface. *Chem. Sci.* **2022**, *13* (13), 3803–3808.
- (17) Nørskov, J. K.; Rossmeisl, J.; Logadottir, A.; Lindqvist, L.; Kitchin, J. R.; Bligaard, T.; Jónsson, H. Origin of the Overpotential for Oxygen Reduction at a Fuel-Cell Cathode. *J. Phys. Chem. B* **2004**, *108* (46), 17886–17892.
- (18) Flores-Leonar, M. M.; Moreno-Esparza, R.; Ugalde-Saldívar, V. M.; Amador-Bedolla, C. Further Insights in DFT Calculations of Redox Potential for Iron Complexes: The Ferrocenium/Ferrocene System. *Comput. Theor. Chem.* **2017**, *1099*, 167–173.
- (19) Steinmann, S. N.; Sautet, P. Assessing a First-Principles Model of an Electrochemical Interface by Comparison with Experiment. *J. Phys. Chem. C* **2016**, *120* (10), 5619–5623.
- (20) Bohra, D.; Chaudhry, J. H.; Burdyny, T.; Pidko, E. A.; Smith, W. A. Modeling the Electrical Double Layer to Understand the Reaction Environment in a CO₂ Electrocatalytic System. *Energy Environ. Sci.* **2019**, *12* (11), 3380–3389.
- (21) Isse, A. A.; Gennaro, A. Electrocatalytic Carboxylation of Benzyl Chlorides at Silver Cathodes in Acetonitrile. *Chem. Commun.* **2002**, No. 23, 2798–2799.
- (22) Isse, A. A.; Lin, C. Y.; Coote, M. L.; Gennaro, A. Estimation of Standard Reduction Potentials of Halogen Atoms and Alkyl Halides. *J. Phys. Chem. B* **2011**, *115* (4), 678–684.
- (23) Isse, A. A.; Scarpa, L.; Durante, C.; Gennaro, A. Reductive Cleavage of Carbon-Chlorine Bonds at Catalytic and Non-Catalytic Electrodes in 1-Butyl-3-Methylimidazolium Tetrafluoroborate. *Phys. Chem. Chem. Phys.* **2015**, *17* (46), 31228–31236.
- (24) Falciola, L.; Gennaro, A.; Isse, A. A.; Mussini, P. R.; Rossi, M. The Solvent Effect in the Electrocatalytic Reduction of Organic Bromides on Silver. *J. Electroanal. Chem.* **2006**, *593* (1–2), 47–56.
- (25) Isse, A. A.; De Giusti, A.; Gennaro, A.; Falciola, L.; Mussini, P. R. Electrochemical Reduction of Benzyl Halides at a Silver Electrode. *Electrochim. Acta* **2006**, *51* (23), 4956–4964.
- (26) Sergeev, A. V.; Chertovich, A. V.; Itkis, D. M.; Sen, A.; Gross, A.; Khokhlov, A. R. Electrode/Electrolyte Interface in the Li-O₂ Battery: Insight from Molecular Dynamics Study. *J. Phys. Chem. C* **2017**, *121* (27), 14463–14469.
- (27) Kislenko, S. A.; Amirov, R. H.; Samoylov, I. S. Effect of Cations on the TiO₂/Acetonitrile Interface Structure: A Molecular Dynamics Study. *J. Phys. Chem. C* **2013**, *117* (20), 10589–10596.
- (28) Sha, M.; Dou, Q.; Luo, F.; Zhu, G.; Wu, G. Molecular Insights into the Electric Double Layers of Ionic Liquids on Au(100) Electrodes. *ACS Appl. Mater. Interfaces* **2014**, *6* (15), 12556–12565.
- (29) Gerlach, T.; Müller, S.; de Castilla, A. G.; Smirnova, I. An Open Source COSMO-RS Implementation and Parameterization Supporting the Efficient Implementation of Multiple Segment Descriptors. *Fluid Phase Equilib.* **2022**, *S60*, 113472.
- (30) Bell, I. H.; Mickoleit, E.; Hsieh, C.-M.; Lin, S.-T.; Vrabec, J.; Breitkopf, C.; Jäger, A. A Benchmark Open-Source Implementation of COSMO-SAC. *J. Chem. Theory Comput.* **2020**, *16* (4), 2635–2646.
- (31) Islam, M. R.; Chen, C.-C. COSMO-SAC Sigma Profile Generation with Conceptual Segment Concept. *Ind. Eng. Chem. Res.* **2015**, *54* (16), 4441–4454.
- (32) Klamt, A. Chapter 6 - The Basic COSMO-RS. In *COSMO-RS*; Klamt, A., Ed.; Elsevier: Amsterdam, 2005; pp 83–107.
- (33) Neese, F.; Wennmohs, F.; Becker, U.; Riplinger, C. The ORCA Quantum Chemistry Program Package. *J. Chem. Phys.* **2020**, *152* (22), 224108.
- (34) Kim, K.; Jordan, K. D. Comparison of Density Functional and MP2 Calculations on the Water Monomer and Dimer. *J. Phys. Chem.* **1994**, *98* (40), 10089–10094.
- (35) Stephens, P. J.; Devlin, F. J.; Chabalowski, C. F.; Frisch, M. J. Ab Initio Calculation of Vibrational Absorption and Circular Dichroism Spectra Using Density Functional Force Fields. *J. Phys. Chem.* **1994**, *98* (45), 11623–11627.
- (36) Becke, A. D. Density-Functional Exchange-Energy Approximation with Correct Asymptotic Behavior. *Phys. Rev. A* **1988**, *38* (6), 3098–3100.
- (37) Vosko, S. H.; Wilk, L.; Nusair, M. Accurate Spin-Dependent Electron Liquid Correlation Energies for Local Spin Density Calculations: A Critical Analysis. *Can. J. Phys.* **1980**, *58* (8), 1200–1211.
- (38) Weigend, F. Accurate Coulomb-Fitting Basis Sets for H to Rn. *Phys. Chem. Chem. Phys.* **2006**, *8* (9), 1057–1065.
- (39) Takano, Y.; Houk, K. N. Benchmarking the Conductor-like Polarizable Continuum Model (CPCM) for Aqueous Solvation Free Energies of Neutral and Ionic Organic Molecules. *J. Chem. Theory Comput.* **2005**, *1* (1), 70–77.
- (40) Warburton, R. E.; Soudackov, A. V.; Hammes-Schiffer, S. Theoretical Modeling of Electrochemical Proton-Coupled Electron Transfer. *Chem. Rev.* **2022**, *122* (12), 10599–10650.
- (41) Medvedev, J. J.; Medvedeva, X. V.; Engelhardt, H.; Klinkova, A. Relative Activity of Metal Cathodes towards Electroorganic Coupling of CO₂ with Benzylic Halides. *Electrochim. Acta* **2021**, *387*, 138528.
- (42) Andrieux, C. P.; Le Gorand, A.; Saveant, J. M. Electron Transfer and Bond Breaking. Examples of Passage from a Sequential to a Concerted Mechanism in the Electrochemical Reductive Cleavage of Arylmethyl Halides. *J. Am. Chem. Soc.* **1992**, *114* (17), 6892–6904.
- (43) Klamt, A. The COSMO and COSMO-RS Solvation Models. *Wiley Interdiscip. Rev. Comput. Mol. Sci.* **2018**, *8* (1), No. e1338.

- (44) Klamt, A. Chapter 5—Statistical Thermodynamics of Interacting Surfaces. In *COSMO-RS*; Klamt, A., Ed.; Elsevier: Amsterdam, 2005; pp 59–81.
- (45) Klamt, A. Chapter 4—Molecular Interactions at the North Pole: A Virtual Experiment. In *COSMO-RS*; Klamt, A., Ed.; Elsevier: Amsterdam, 2005; pp 49–58.
- (46) Van Der Spoel, D.; Lindahl, E.; Hess, B.; Groenhof, G.; Mark, A. E.; Berendsen, H. J. C. GROMACS: Fast, Flexible, and Free. *J. Comput. Chem.* **2005**, *26* (16), 1701–1718.
- (47) Hess, B.; Kutzner, C.; van der Spoel, D.; Lindahl, E. GROMACS 4: Algorithms for Highly Efficient, Load-Balanced, and Scalable Molecular Simulation. *J. Chem. Theory Comput.* **2008**, *4* (3), 435–447.
- (48) Vaitkus, A.; Merkys, A.; Gražulis, S. Validation of the Crystallography Open Database Using the Crystallographic Information Framework. *J. Appl. Crystallogr.* **2021**, *54* (2), 661–672.
- (49) Spreadborough, J.; Christian, J. W. High-Temperature X-Ray Diffractometer. *J. Sci. Instrum.* **1959**, *36* (3), 116–118.
- (50) Kowsari, M. H.; Tohidifar, L. Systematic Evaluation and Refinement of Existing All-Atom Force Fields for the Simulation of Liquid Acetonitrile. *J. Comput. Chem.* **2018**, *39* (23), 1843–1853.
- (51) Sambasivarao, S. V.; Acevedo, O. Development of OPLS-AA Force Field Parameters for 68 Unique Ionic Liquids. *J. Chem. Theory Comput.* **2009**, *5* (4), 1038–1050.
- (52) Zhu, A.; Zhang, X.; Liu, Q.; Zhang, Q. A Fully Flexible Potential Model for Carbon Dioxide. *Chin. J. Chem. Eng.* **2009**, *17* (2), 268–272.
- (53) Jorgensen, W. L.; Maxwell, D. S.; Tirado-Rives, J. Development and Testing of the OPLS All-Atom Force Field on Conformational Energetics and Properties of Organic Liquids. *J. Am. Chem. Soc.* **1996**, *118* (45), 11225–11236.
- (54) Houndonougbo, Y.; Laird, B. B.; Kuczera, K. Transport Properties of CO₂-Expanded Acetonitrile from Molecular Dynamics Simulations. *J. Chem. Phys.* **2007**, *126* (7), 074507.
- (55) Heinz, H.; Vaia, R. A.; Farmer, B. L.; Naik, R. R. Accurate Simulation of Surfaces and Interfaces of Face-Centered Cubic Metals Using 12–6 and 9–6 Lennard-Jones Potentials. *J. Phys. Chem. C* **2008**, *112* (44), 17281–17290.
- (56) Hauner, J.; Bühlmeier, H.; Steffen, J.; Trzeciak, S.; Taccardi, N.; Wasserscheid, P.; Zahn, D.; Göring, A.; Libuda, J. Temperature-Dependent Structure Formation in the Wetting Layer of the Ionic Liquid [C₂C₁Im]⁺[OTf][−] on Au(111). *J. Phys. Chem. C* **2024**, *128* (9), 3894–3906.
- (57) Bhattacharyya, A.; Tiwari, V.; Karmakar, T. Electrostatic-Driven Self-Assembly of Janus-like Monolayer-Protected Metal Nanoclusters. *J. Phys. Chem. Lett.* **2024**, *15* (3), 687–692.
- (58) Murke, S.; Chen, W.; Pezzotti, S.; Havenith, M. Tuning Acid-Base Chemistry at an Electrified Gold/Water Interface. *J. Am. Chem. Soc.* **2024**, *146*, 12423–12430.
- (59) Wang, M.; Ni, S.-D.; Yin, Y.-W.; Ma, Y.-Q.; Ding, H.-M. Molecular Modeling of the Fluorination Effect on the Penetration of Nanoparticles across Lipid Bilayers. *Langmuir* **2024**, *40* (2), 1295–1304.
- (60) Zhao, H.; Yang, Y.; Shu, X.; Qiao, M.; Dong, L.; Ran, Q. Computational Simulations of Adsorption Behavior of Anionic Surfactants at the Portlandite-Water Interface under Sulfate and Calcium Ions. *Langmuir* **2024**, *40* (7), 3911–3922.
- (61) Feng, G.; Huang, J.; Sumpter, B. G.; Meunier, V.; Qiao, R. Structure and Dynamics of Electrical Double Layers in Organic Electrolytes. *Phys. Chem. Chem. Phys.* **2010**, *12* (20), 5468–5479.
- (62) Zare, M.; Saleheen, M. S.; Singh, N.; Uline, M. J.; Faheem, M.; Heyden, A. Liquid-Phase Effects on Adsorption Processes in Heterogeneous Catalysis. *JACS Au* **2022**, *2* (9), 2119–2134.
- (63) Hess, B.; Bekker, H.; Berendsen, H. J. C.; Fraaije, J. G. E. M. LINCS: A Linear Constraint Solver for Molecular Simulations. *J. Comput. Chem.* **1997**, *18* (12), 1463–1472.
- (64) Luo, Y.-R. *Comprehensive Handbook of Chemical Bond Energies*; CRC Press: Boca Raton, 2007.
- (65) Markovits, A.; Minot, C. Theoretical Study of the Acetonitrile Flip-Flop with the Electric Field Orientation: Adsorption on a Pt(111) Electrode Surface. *Catal. Lett.* **2003**, *91* (3/4), 225–234.
- (66) Baldelli, S.; Mailhot, G.; Ross, P.; Shen, Y.-R.; Somorjai, G. A. Potential Dependent Orientation of Acetonitrile on Platinum (111) Electrode Surface Studied by Sum Frequency Generation. *J. Phys. Chem. B* **2001**, *105* (3), 654–662.
- (67) Ludwig, T.; Singh, A. R.; Nørskov, J. K. Acetonitrile Transition Metal Interfaces from First Principles. *J. Phys. Chem. Lett.* **2020**, *11* (22), 9802–9811.
- (68) Marcus, R. A. Symmetry or Asymmetry of k_{ET} and iSTMvs. Potential Curves. *J. Chem. Soc., Faraday Trans.* **1996**, *92* (20), 3905–3908.
- (69) Bard, A. J.; Faulkner, L. R. *Electrochemical Methods: Fundamentals and Applications*, 2nd ed.; Wiley, 2001.
- (70) Henstridge, M. C.; Laborda, E.; Compton, R. G. Asymmetric Marcus-Hush Model of Electron Transfer Kinetics: Application to the Voltammetry of Surface-Bound Redox Systems. *J. Electroanal. Chem.* **2012**, *674*, 90–96.
- (71) Lan, J.; Kapil, V.; Gasparotto, P.; Ceriotti, M.; Iannuzzi, M.; Rybkin, V. V. Simulating the Ghost: Quantum Dynamics of the Solvated Electron. *Nat. Commun.* **2021**, *12* (1), 766.
- (72) Rybkin, V. V. Mechanism of Aqueous Carbon Dioxide Reduction by the Solvated Electron. *J. Phys. Chem. B* **2020**, *124* (46), 10435–10441.
- (73) Johnson, E. F.; Boutin, E.; Haussener, S. Surface Charge Boundary Condition Often Misused in CO₂ Reduction Models. *J. Phys. Chem. C* **2023**, *127* (37), 18784–18790.
- (74) Yang, W.; Kalavalapalli, T. Y.; Krieger, A. M.; Khvorost, T. A.; Chernyshov, I. Yu.; Weber, M.; Uslamin, E. A.; Pidko, E. A.; Filonenko, G. A. Basic Promoters Impact Thermodynamics and Catalyst Speciation in Homogeneous Carbonyl Hydrogenation. *J. Am. Chem. Soc.* **2022**, *144* (18), 8129–8137.
- (75) Kuliaev, P. O.; Pidko, E. A. Operando Modeling of Multi-component Reactive Solutions in Homogeneous Catalysis: From Non-Standard Free Energies to Reaction Network Control. *ChemCatChem* **2020**, *12* (3), 795–802.
- (76) Bao, D.; Millare, B.; Xia, W.; Steyer, B. G.; Gerasimenko, A. A.; Ferreira, A.; Contreras, A.; Vullev, V. I. Electrochemical Oxidation of Ferrocene: A Strong Dependence on the Concentration of the Supporting Electrolyte for Nonpolar Solvents. *J. Phys. Chem. A* **2009**, *113* (7), 1259–1267.
- (77) Seto, K.; Nakayama, T.; Uno, B. Formal Redox Potentials of Organic Molecules in Ionic Liquids on the Basis of Quaternary Nitrogen Cations as Adiabatic Electron Affinities. *J. Phys. Chem. B* **2013**, *117* (37), 10834–10845.
- (78) Qu, X.; Persson, K. A. Toward Accurate Modeling of the Effect of Ion-Pair Formation on Solute Redox Potential. *J. Chem. Theory Comput.* **2016**, *12* (9), 4501–4508.
- (79) Mugisa, J.; Chukwu, R.; Brogioli, D.; La Mantia, F. Effect of Ion-Pairing on the Kinetics of Redox Systems with Concentrated Supporting Electrolyte. *Electrochim. Acta* **2024**, *473*, 143473.
- (80) Duan, A.; Wang, Z.; Huang, X.; Li, Y. Anion-Dependent Redox Chemistry of p-Type Poly(Vinylidimethylphenazine) Cathode Materials. *Angew. Chem.* **2023**, *135* (24), No. e202302754.